ISIJ International, Vol. 44 (2004), No. 7, pp. 1180–1187

Mechanical Properties of Thin Wall Ductile Iron-Influence of Carbon Equivalent and Graphite Distribution

P. DAVID, J. MASSONE,[1)] R. BOERI[1)] and J. SIKORA[1)]

Graduate Student, Metallurgy Division, INTEMA, National University of Mar del Plata, FONCYT, Av. Juan B. Justo 4302-B7608 FDQ Mar del Plata, Argentina. 1) Faculty of Engineering, Metallurgy Division INTEMA, National University of Mar del Plata, CONICET, Av. Juan B. Justo 4302-B7608FDQ Mar del Plata, Argentina. E-mail: jsikora@fi.mdp.edu.ar

(*Received on January 5, 2004; accepted in final form on April 11, 2004*)

This work focuses on the study of the mechanical properties and microstructure of plates of thin wall ductile iron, cast in sand moulds of vertical and horizontal configuration. All tests were carried out on ferritised samples. Melts of carbon equivalent values ranging from 4.06 to 4.85 were used to cast plates of thickness ranging from 1.5 to 4 mm. The results show that irons having carbon equivalent values greater than 4.6 exhibit a marked tendency to develop exploded graphite shapes and agglomeration of graphite nodules. As a result, these irons show scattered values of mechanical properties. As irons are produced with carbon equivalent values below 4.6 %, the mechanical properties improve, reaching levels that satisfy the requirements of standards developed for ferritised ductile irons sand cast in Y-blocks.

KEY WORDS: ductile iron; thin wall; mechanical properties; deteriorated graphite; carbon equivalent.

1. Introduction

Design engineers, vehicle makers and foundrymen are among those members of the engineering community that are more strongly pressed to produce lighter, stronger and stiffer metallic parts. Ductile iron can be a material of choice to produce such parts, since it is suited to produce cast parts of complex shape, it can reach very high strength through heat treatment, and it is relatively inexpensive. Compared to cast aluminium alloys, ductile iron shows much higher elastic modulus, a comparable strength to density ratio, better fatigue strength, and lower production cost. Nevertheless, to make full use of its relative advantages to produce light parts, ductile iron must be cast with thin walls. Conventional technology limits the minimum thickness of DI parts to about 5 mm. Nevertheless, the study of the production of thinner parts is receiving increasing attention. Reducing the minimum production thickness of DI allows to design and cast hollow parts of high stiffness.[1)] Nevertheless, as the thickness of the parts diminishes, the metallurgical quality of the DI becomes increasingly critical. Microstructural anomalies and structural defects, such as microshrinkage or defective skin, graphite alignment, oriented dendrites, inverse chill, oxide films and particles and flake graphite rim, decrease mechanical properties.[2)]

Some of the first issues to be dealt with in order to make it possible the production of thin wall ductile iron (TWDI) are i) Proper mould design to allow for the production of sound parts in spite of the rapid cooling rate and the consequently reduced fluidity. Software for numerical simulation of mould filling and solidification has proven to be an excellent tool to assist in this task. ii) Proper conditioning of the melt before pouring, so as to obtain homogeneous and carbide free microstructures. This is the subject that has received more attention in the literature.[2–5)] Most studies concluded that high carbon equivalent (CE) irons must be used to avoid as-cast carbide precipitation. Carbides decrease the strength, ductility and machinability of TWDI. Early work of Loper (1969) showed that an increase in CE causes an increase in the nodule count and a significant decrease in the precipitation of carbides. Loper indicated that CE must be raised to 4.75 to 4.92% in order to obtain carbide free structures in 3 to 5 mm thickness sand cast DI. More recently, studies carried out on DI containing lower levels of Mn, P and S recommended to adopt a CE=4.72% (3.7% C and 3.4% Si) for carbide-free SG iron in castings with wall thickness 3 mm and this is consistent with the recommendation of QIT, that estimates the required CE using the equation $CE=4.9265-0.0425 \cdot t$, where t is the thickness (sand cast).[3)]

Javaid[4,5)] reports that carbide free 3 mm thick DI plates were obtained in sand moulds by using DI having CE ranging from 4.5 to 5.08%.

Laberque[6)] used special inoculants, having Bi and Ce, to obtain carbide free microstructures in 3 mm thick plates cast of 4.6 to 4.9% CE ductile iron. O. Dógan[7)] used DI of CE ranging from 4.7 to 4.8% to cast carbide free plates of thickness ranging from 1.5 to 9 mm, using independent and connected plates in a horizontal mould.

The review of the literature shows that the use of hypereutectic DI, with CE ranging from 4.45 to 4.9%, is recommended when plates of thickness below 5 mm are to be cast free from carbides in sand moulds.

Recent studies of the authors[8)] showed that ledeburitic

carbides precipitated in TWDI in large amounts can be easily dissolved by a short austenitizing heat treatment. Therefore, this investigation was not focused on the attainment of carbide free structures as cast.

Several studies focused on the mechanical properties of TWDI.[2,3,9–11] Most authors make use of the quality index proposed by Loper and Kotschi,[12] to assess the quality of the TWDI parts tested. A baseline is defined on tensile strength *vs.* elongation and yield strength *vs.* elongation plots. The quality of a given iron is judged to be better as the points, defined by its tensile strength, yield strength and elongation, lie more above the baseline.

Stefanescu *et al.*[2] report that the tensile strength and elongation of TWDI vary within a large range. This variability in the results of tensile testing seems to be caused by microstructural anomalies generated during solidification, such as micro-shrinkage, graphite and dendrite aligning, inverse chill, oxide particles, and by some morphological factors, such as the surface roughness of the samples. When properties are measured on sound TWDI plates, free from internal defects and carbides, samples of mainly ferritic matrix show tensile strength of 413–482 MPa, yield strength of 296–317 MPa, and 18–25% elongation, for hardness ranging between 133 and 167 HB. Samples of pearlitic–ferritic matrix show 606–758 MPa Tensile strength, 400–482 MPa yield strength, 6–12% elongation and 210–240 HB hardness.

In other study, Stefanescu *et al.*[3] show that the strength and elongation of TWDI are largely influenced by the surface roughness and the graphite morphology. Poor properties of TWDI are associated to low nodularity and coarse roughness. Testing of samples including the original casting skin shows that as roughness values exceed Ra=10 μm, a pronounced decrease in strength and elongation is observed. Samples in which the casting skin has been removed by grinding show consistently higher tensile properties.

Labrecque and Gagné[9] measured the mechanical properties of ductile irons cast in sections of 3 and 10 mm. The results of tensile strength and elongation show that the samples taken from the 10 mm plates satisfy the minimum quality index, while samples from the 3 mm plates show lower and more disperse values, that fail to satisfy the standards in most cases.

Javaid and Davis[10] also measured mechanical properties of TWDI, and found disperse values. Good mechanical properties, satisfying ASTM A 536, were obtained when the material showed good nodularity, high nodule counts and a matrix free from carbides and inclusions. Samples that failed to satisfy the standards showed microstructural anomalies. In general, it was found that lower elongation reflects lower Si (higher pearlite contents), the presence of carbides, or lower nodule count or nodularity, while higher elongation is shown by irons of higher Si (higher ferrite contents), improved nodularity and higher nodule count.

In summary, the results of the literature indicate that TWDI has the potential to satisfy the requirements of the standards devised for regular DI, nevertheless, disperse values were found in many studies, with a significant proportion of samples that fail to satisfy the minimum requirements of ASTM A 536. Unsatisfactory properties were generally linked to casting defects. In most studies, mechanical properties have been measured on as-cast samples. Under this conditions, samples of different thickness will have different matrix microstructure, and therefore different mechanical properties. Then, direct comparison of the mechanical properties of samples taken from sections of different thickness is not possible. A systematic study of the factors controlling the presence of defects on TWDI parts is therefore necessary to ensure that satisfactory properties can be consistently obtained in industrial production.

The objectives of this investigation are to study the mechanical properties of ferritic TWDI plates cast in sand moulds, and to identify the effect of the morphology, count and distribution of the graphite phase particles, and the carbon equivalent on the tensile properties.

2. Experimental Methods

The melts used in this investigation were produced at the foundry pilot plant of INTEMA, using a 50 kg medium frequency induction furnace. The charge was made of ductile iron grade pig iron, steel scrap, FeSi and a carburising agent. Several melts having carbon equivalents (CE) ranging from 4.06 to 4.85% were poured. All melts were heated to 1 540–1 550°C before treatment. The melt was treated in two stages, using separate ladles. Nodularising was carried out by applying the sandwich method in the first ladle, and using FeSiMg (6%). Inoculation was carried out in the second ladle by using FeSi (75% Si, 1.1% Ca) in the stream.

The temperature of the melt in the ladle was measured immediately before pouring the moulds. Pouring temperature was between 1 340 and 1 360°C in all cases.

Two different moulds were used to obtain thin plates of DI. **Figure 1** shows a horizontal mould that provides plates of 1.5, 2, 3 and 4 mm of thickness. **Figure 2** shows a vertical mould designed to yield two plates of 2 and 4 mm of thickness. Both moulds are designed to provide DI plates large enough to make tensile test specimens. The moulds were made by using AFS-60 silica sand and 1 wt% alkydic resin as a binder.

Since the main objective of this study is to analyse the influence of the graphite shape, size and distribution on the mechanical properties, it seemed necessary to obtain a similar matrix microstructure in all samples, regardless CE

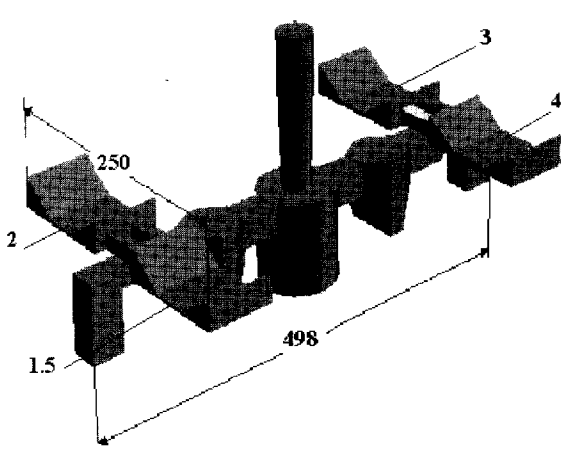

Fig. 1. Horizontal casting (dimensions in millimetres).

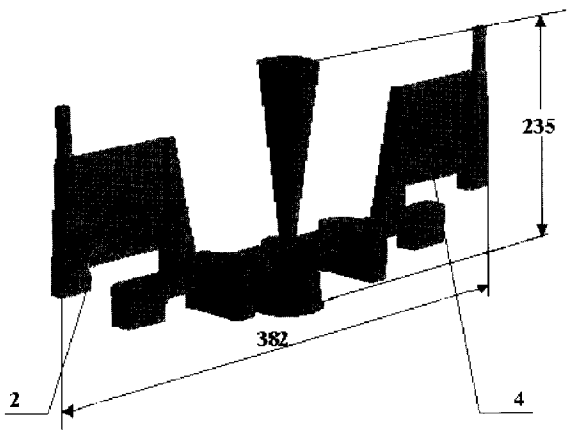

Fig. 2. Vertical casting (dimensions in millimetres).

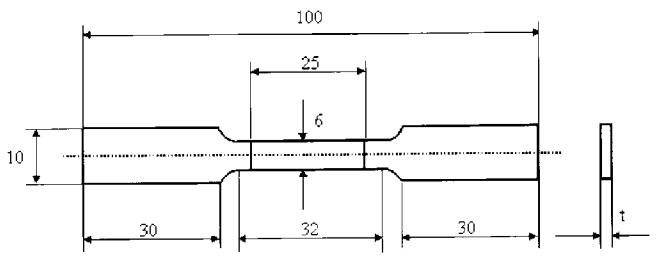

Fig. 3. Schema of the tensile test samples (dimensions in millimetres).

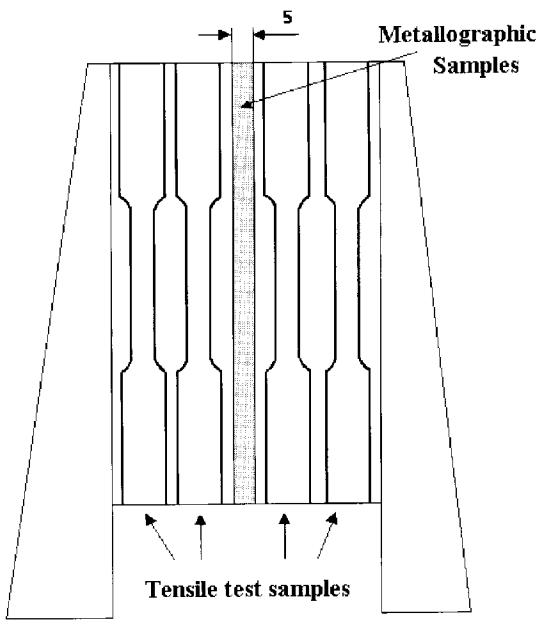

Fig. 4. Mechanical properties testing sample and metallographic sample.

and section thickness. Therefore, all parts were ferritised after casting, to obtain a fully ferritic matrix in all cases. This was done before machining by austenitising al 930°C during 2 h, followed by furnace cooling. All samples surfaces were ground to remove the casting skin. Tensile tests were carried out using an Instron 8501. Ultimate Tensile Strength (UTS), yield strength (SY0.2) and elongation (e_f) were measured according to standard ASTM E 8M-95a on flat samples. **Figure 3** shows the dimensions of the tensile test samples used. **Figure 4** shows the way in which tensile and metallographic samples are taken from the TWDI

Table 1. Chemical composition of the melts.

Chemical Composition (Wt%)								
Melt	C	Si	Mn	S	P	Mg	CE	Symbol in plots
A	3.70	3.26	0.28	0.02	0.06	0.059	**4.78**	◆
B	3.65	3.59	0.27	0.03	0.03	0.021	**4.85**	◇
C	3.80	2.92	0.27	0.02	0.04	0.040	**4.77**	■
D	3.53	2.89	0.32	0.07	0.05	0.052	**4.49**	▲
E	3.65	3.04	0.20	0.04	0.05	0.048	**4.65**	x
F	3.46	2.85	0.18	0.02	0.05	0.029	**4.41**	+
G	3.60	2.72	0.23	0.01	0.04	0.040	**4.51**	○
H	3.60	3.15	0.20	0.01	0.04	0.032	**4.65**	-
I	3.19	2.63	0.21	0.02	0.03	0.030	**4.06**	●

plates cast using the vertical mould.

The characterisation of the microstructure of the DI parts was done after regular polishing. An Olympus PMG-3 microscope was used. In order to obtain a characterisation of the microstructure that represents the tested material as closely as possible, the metallographic specimens were taken from the calibrated section of the tensile samples after testing. Quantitative metallography was made by using routines developed for the software Image Pro Plus. Digital images were obtained by using an STC-60 video camera and a PV-CL544XPII video board. Nodule counts were measured on un-etched samples The threshold value for the size of the particles that are counted as graphite nodules was set to 5 μm. The content of carbides was measured on samples taken from the location shown in Fig. 4, after etching with ammonia persulfate. Values reported are the average of three measurements per sample.

The graphite morphology (nodularity) was characterised by measuring the sphericity[13] on the 2 and 4 mm plates from the vertical mould. Sphericity (Sph) values were calculated from values of area and perimeter of nodules measured using image analysis. A threshold value of 5 μm was used for the diameter of the particles accounted as nodules. Sph was calculated using the following expression:

$$\mathrm{Sph} = \frac{4 \cdot \pi \cdot \mathrm{Area}}{\mathrm{Perimeter}^2}$$

3. Results

3.1. Chemical Composition

Table 1 lists the denomination and chemical composition of the melts used. The table also shows the symbol used to identify data from each melt in all the plots and graphs. The different melts aimed to cover a wide range of CE values by adjusting contents of C and Si.

3.2. Nodule Counts

Figures 5 and **6** show the average nodule counts of plates of 2 and 4 mm of thickness cast using the vertical and the horizontal moulds. As the thickness of the plate diminishes, the nodule count increases largely, as a result of the faster cooling rate. The 2 mm plate of the vertical mould shows higher nodular counts than a similar plate taken from the horizontal mould. This effect is not seen on the 4 mm plates.

3.3. Graphite Morphology and Distribution

Table 2 lists the values of Sph and optical Nodularity. In al cases, both Sph and Nodularity values are high, and they improve as the thickness of the plate becomes smaller.

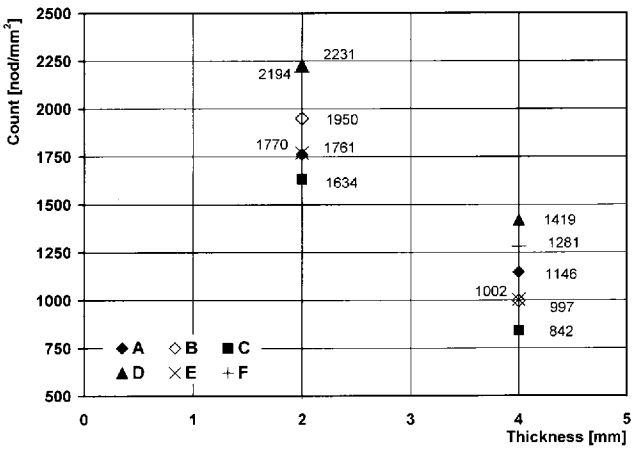

Fig. 5. Nodule counts for 2 and 4 mm plates of the vertical mould.

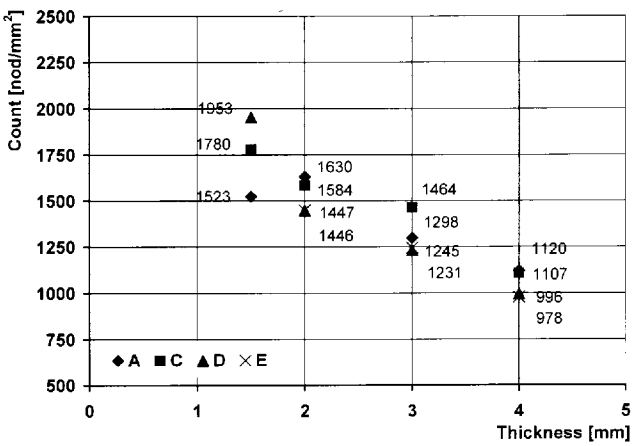

Fig. 6. Nodule counts the 1.5, 2, 3 and 4 mm plates of the horizontal mould.

Table 2. Sphericity and visual nodularity of vertical mould samples.

Melt	Sphericity		Visual Nodularity [%]	
	2 mm	4 mm	2 mm	4 mm
A	0.66	0.62	100**	90**
B	0.65	0.51	90*	80/70*
C	0.69	0.59	100**	90**
D	0.67	0.65	100	90/80
E	0.74	0.72	100	100/90
F	0.72	0.69	100	100

* Clusters of nodules and exploded graphite.
** Exploded graphite.

Highly hypereutectic irons (A, B and C) show exploded graphite. Careful analysis of a large number of fields shows that an homogeneous distribution of evenly sized graphite nodules is observed in the nearly eutectic composition melts. As the CE value of the melt increases the presence of pro-eutectic graphite nodules becomes evident. Pro-eutectic nodules can be identified since they are larger and are present in smaller amount than eutectic nodules. This can be verified in samples of plates of all the thickness values investigated. Additionally, as the number and size of pro-eutectic graphite nodules increase, the presence of clusters of nodules and exploded graphite becomes characteristic. **Figure** 7(a) shows a low magnification mapping of the graphite distribution on a grid of points of a 4 mm thick plate of Melt C (CE: 4.77%), and magnifications of select-

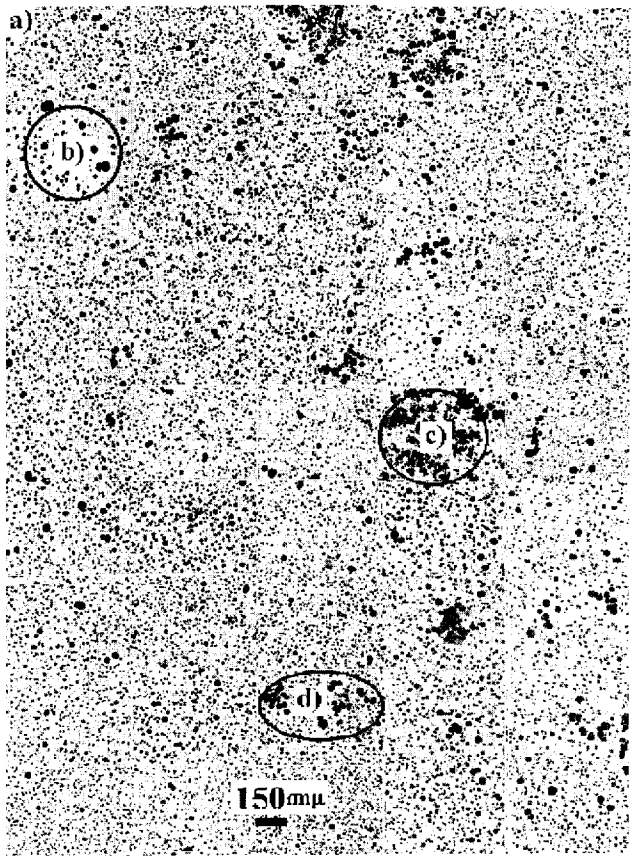

Fig. 7a. Mapping of the microstructure of a 4 mm plate, (melt C).

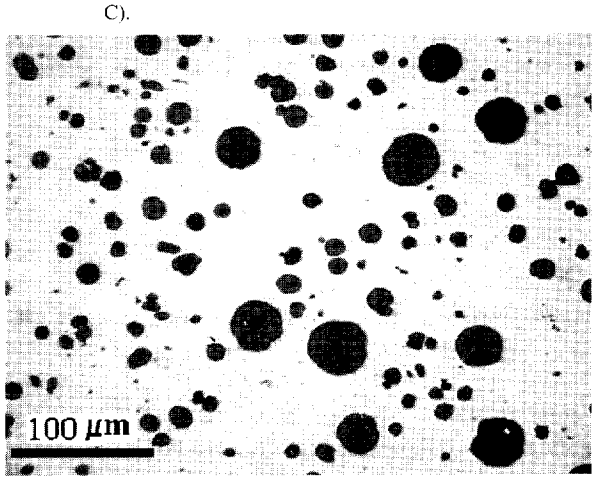

Fig. 7b. Area of homogeneous graphite distribution from Fig. 7(a).

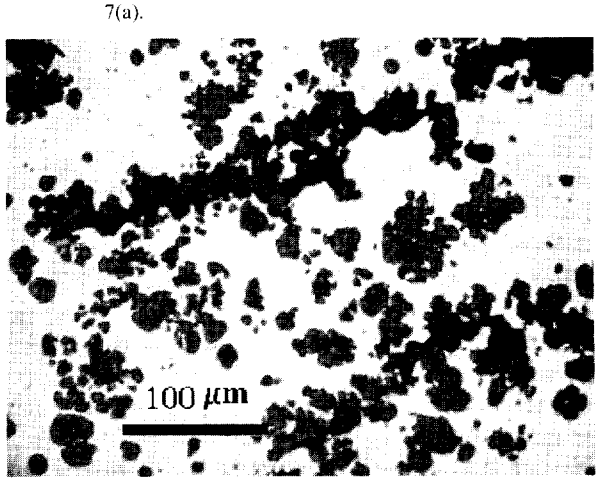

Fig. 7c. Area of exploded nodules from Fig. 7(a).

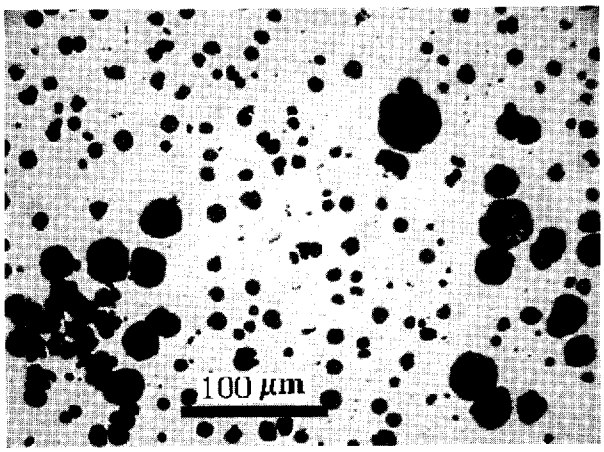

Fig. 7d. Area of nodule clusters from Fig. 7(a).

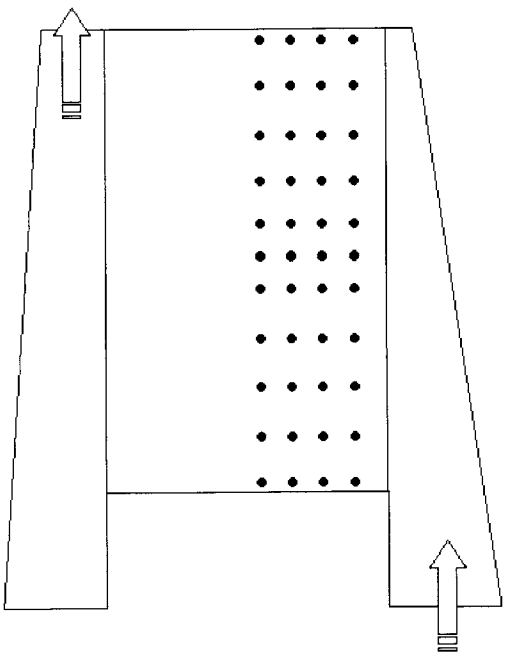

Fig. 8. Scheme of the 4 mm vertical plate indicating the points for metallography study, (melt C).

ed areas of the polished surface. The points at which the metallographies shown in Fig. 7(a) are taken are shown in **Fig. 8**. Large areas of the sample show relatively homogeneous graphite distribution, as shown in Fig. 7(b) where a large amount of spherically shaped nodules of about 10 μm of diameter, and a smaller amount of larger nodules of about 25 μm in diameter are observed. Nevertheless, other surface areas show areas of exploded nodules (Fig. 7(c)) and nodule clusters (Fig. 7(d)).

A careful analysis of the metallographies of all samples indicates that the presence of large pro-eutectic graphite nodules becomes noticeable as the CE value exceeds 4.6%. No graphite clustering or exploded graphite nodules were observed in melts of CE below 4.5%.

Figures 9 and **10** show the fracture surface of tensile samples observed by a Scanning Electron Microscope. Graphite clusters and exploded graphite are seen on the fracture surface, what suggests that these anomalies of the graphite microstructure act as stress concentrators and promote fracture.

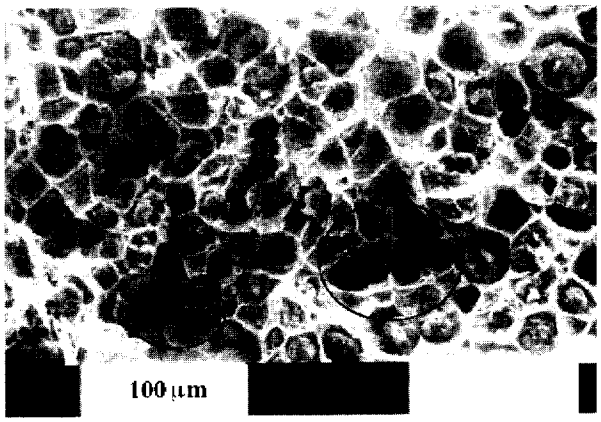

Fig. 9. SEM image of graphite clusters from the fracture surface of tensile samples.

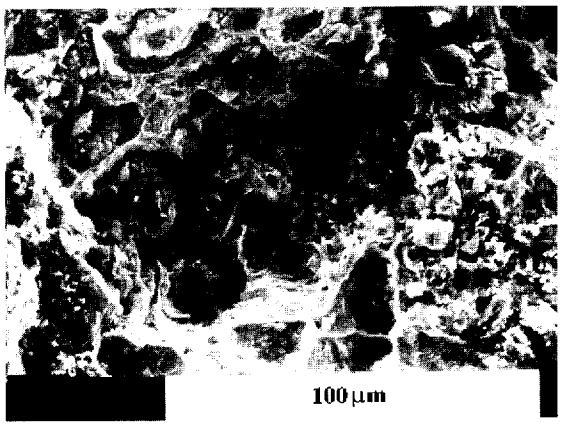

Fig. 10. SEM image of exploded graphite from the fracture surface of tensile samples.

A detrimental factor commonly related to the use of hypereutectic DI is the possible flotation of graphite. This effect is generally more noticeable as the thickness of the parts increase. In the present case, graphite flotation should not be a problem since the sections used are very small. Nevertheless, the fact that large pro-eutectic nodules showed tendency to form clusters suggested that these nodules could be present in the melt very early, an therefore they could be dragged by the metal streams, forcing them to cluster into locations in which different streams interact or end. If this mechanism was operating, dragged nodules should be present, for example, at the top of the vertical plates. Careful examination of the microstructure at such location of plates of melts of CE greater than 4.65% show no evidence of graphite flotation, but clustering of hypereutectic graphite nodules is found extensively on the higher CE melts, as shown in Fig. 7, **Fig. 11** and **Fig. 12**. This suggests that even though hypereutectic nodules form, they are not able to float to the point that they reach the upper surfaces of the plates. Instead, the hypereutectic nodules precipitated in the melt seem to cluster together at locations throughout the sample.

3.4. Amount and Distribution of As-cast Carbides

As pointed out above, all carbides precipitated during solidification were dissolved by a ferritising treatment. Nevertheless, the information regarding amount and distrib-

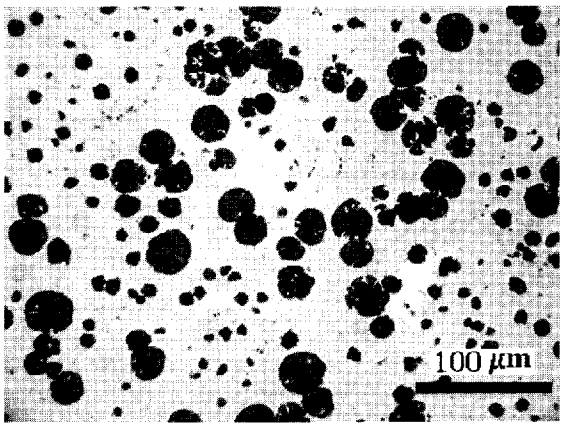

Fig. 11. Microestructure of tensile samples from 4 mm vertical plates showing graphite clusters (melt C).

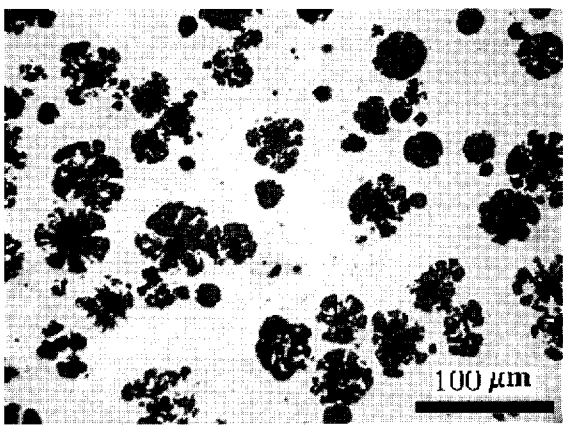

Fig. 12. Microestructure of tensile samples from 4 mm vertical plates, showing exploded graphite (melt C).

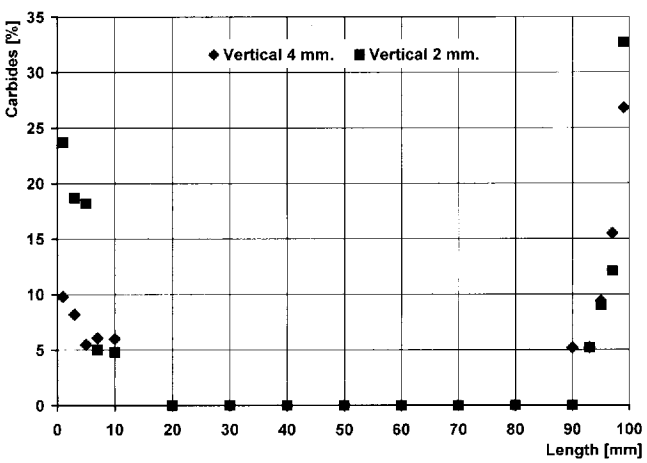

Fig. 13. Carbides content along the centre line of the 2 and 4 mm vertical plates (melt D).

ution of carbides along the thin plates was considered to be useful, and was therefore measured. **Figure 13** shows the amount of carbides present in the 2 and 4 mm thick vertical plates of melt D, measured along the vertical line shown in Fig. 4. Although noticeable amounts of carbides are present at the bottom and top of the plates, most of the volume of the plates appears free from carbides. This indicates that there is an edge effect, since the top and bottom of the vertical plates cool down very fast, as thin protuberances or fins.

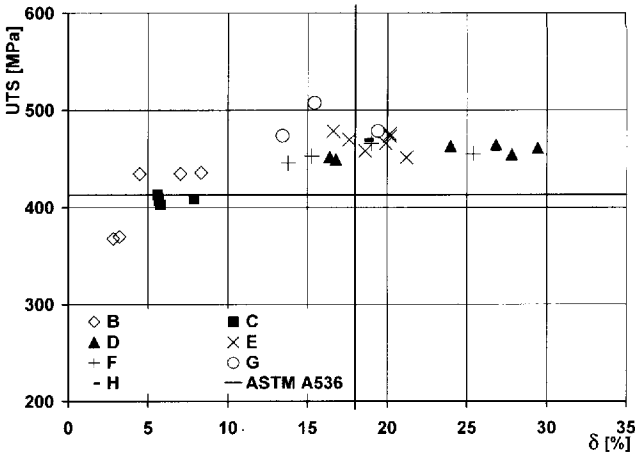

Fig. 14. Ultimate tensile strength *vs.* elongation measured on samples taken from 2 mm plates of the vertical mould.

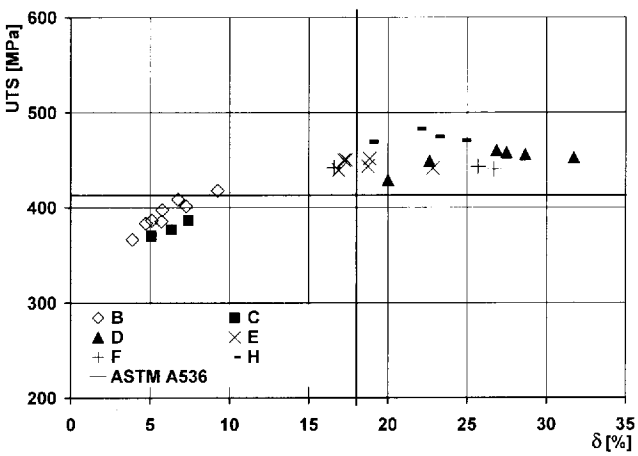

Fig. 15. Ultimate tensile strength *vs.* elongation measured on samples taken from 4 mm plates of the vertical mould.

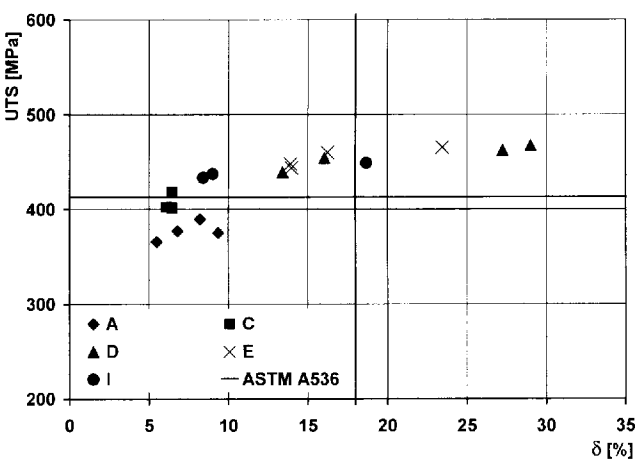

Fig. 16. Ultimate tensile strength *vs.* elongation measured on samples taken from 2 mm plates of the horizontal mould.

4. Mechanical Propeties

4.1. Tensile Tests

Figures 14 to **18** show the UTS and elongation measured on samples taken from plates cast using the vertical and horizontal moulds. The lines show the minimum properties

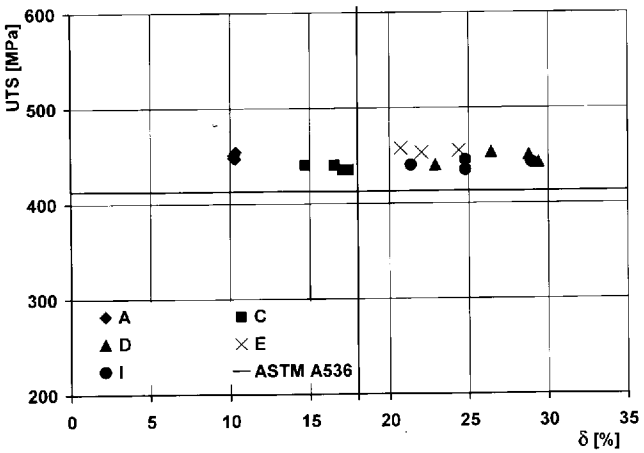

Fig. 17. Ultimate tensile strength *vs.* elongation measured on samples taken from 3 mm plates of the horizontal mould.

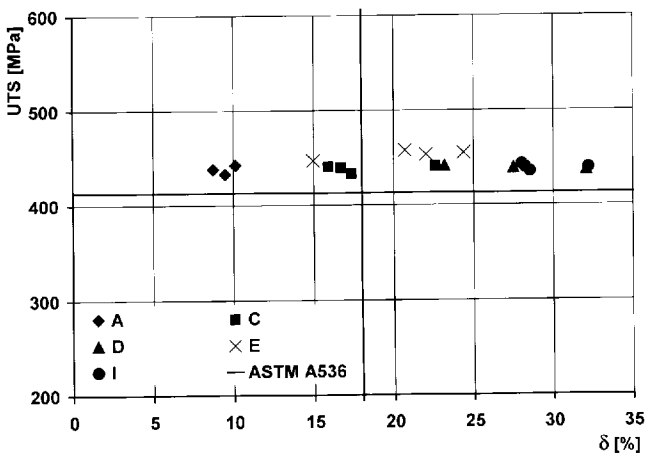

Fig. 18. Ultimate tensile strength *vs.* elongation measured on samples taken from 4 mm plates of the horizontal mould.

of DI defined in standard ASTM A536 (grade 60-40-18, annealed) for tensile samples taken from standardised Y-blocks. Figure 14 shows that most tensile samples from the 2 mm plates satisfy the minimum strength, but more than half fail to satisfy the required elongation. Figure 15 shows the results of tensile testing of the 4 mm plates. In this case a larger proportion of samples give satisfactory properties. It is important to note that for both 2 and 4 mm plates, most of the samples showing unsatisfactory properties came from the highly hypereutectic melts (B and C).

Figures 16 to 18 show the values of UTS and elongation for samples taken from the horizontal moulds. As in the vertical mould samples, some tests samples surpass the minimum specifications of ASTM A536, in particular for the 3 and 4mm thick plates. As in the case of vertical moulds, the samples of the highly hypereutectic irons A, B and C generally show low elongation values. Figures 14 through 18 show that for the larger elongation values, the UTS remains approximately constant as the elongation increases. This is caused by the small hardening coefficient of the ferritic DI, that allows relatively large deformations of the sample without a noticeable increase in strength.

All plates were carefully examined to identify the possible presence of shrinkage porosity. The results indicate that

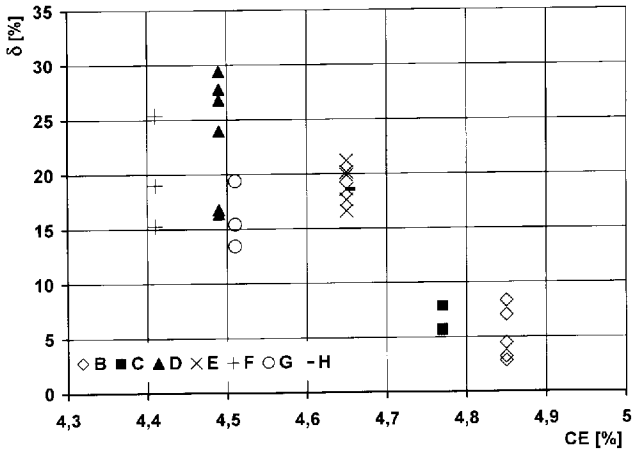

Fig. 19. C.E *vs.* elongation measured on samples taken from 2 mm plates of the vertical mould.

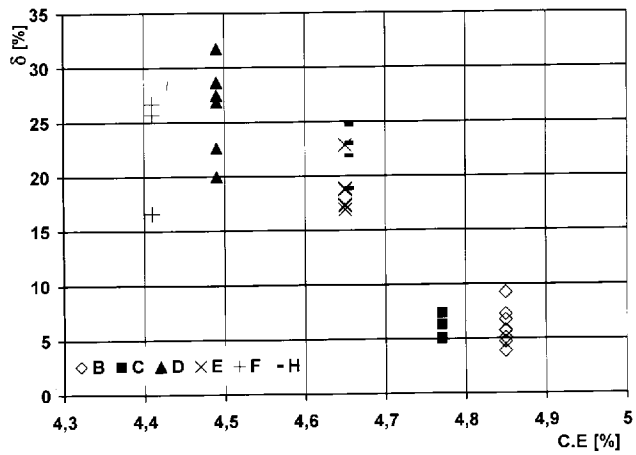

Fig. 20. C.E *vs.* elongation measured on samples taken from 4 mm plates of the vertical mould.

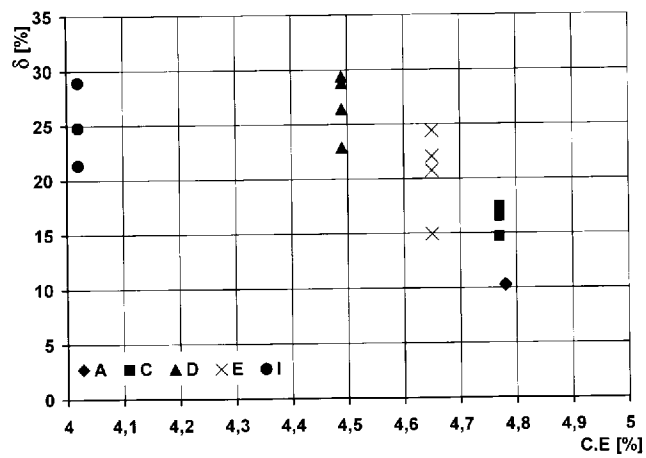

Fig. 21. C.E *vs.* elongation measured on samples taken from 3 mm plates of the horizontal mould.

there is no shrinkage porosity on the samples, and therefore this is not the cause of the lower elongation values measured on the highly hypereutectic irons.

4.2. Influence of CE on the Elongation, Tensile Strength and Yield Strength

Figures 19 to **22** show the influence of CE on the elon-

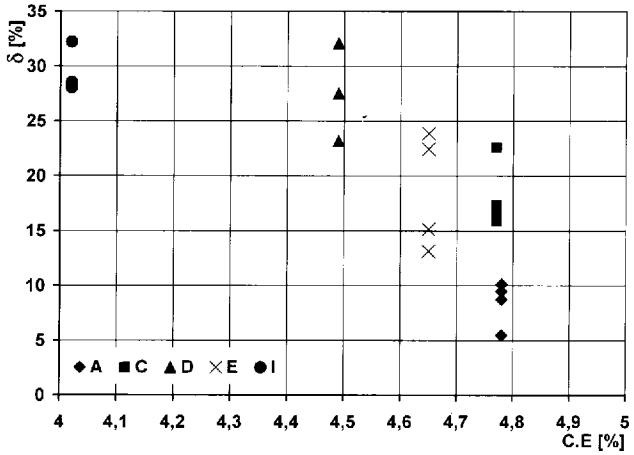

Fig. 22. C.E *vs.* elongation measured on samples taken from 4 mm plates of the horizontal mould.

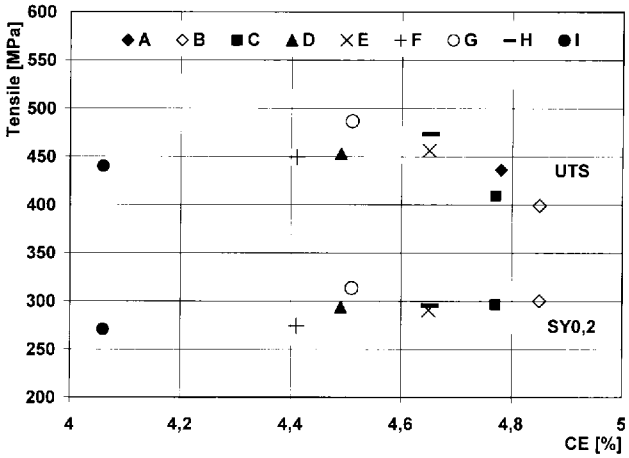

Fig. 23. Ultimate tensile strength and yield strength *vs.* C.E measured on samples of the horizontal and vertical moulds.

gation of plates of different thickness. For samples of both vertical and horizontal moulds, the results consistently indicate that the elongation is larger for the lower CE melts. In particular, most samples of melts of CE<4.6% satisfy the minimum elongation for ferritic grades of DI.

This observation about the influence of CE on elongation, together with the observation discussed on Sec. 3.3, that stated that nodule clustering and nodule explosion takes place preferentially for the higher CE melts, suggests that the observed lower average elongation in the higher CE melts is caused by graphite defects.

This was verified by carefully examination on fracture surface of those tensile samples showing lower elongation, using scanning electron microscope. In all cases graphite clusters or regions of exploded graphite were present at the surface. Since it has been shown in Sec. 3.3 that the occurrence of such deteriorated graphite shapes is not generalised, but confined to some locations, the fact that all fracture surfaces include such graphite anomalies suggest that they are playing a key role, decreasing significantly the elongation.

An analysis of the data on elongation shows that even in those melts for which CE is below 4.6%, the values of elongation show a dispersion somehow larger than that observed on samples of regular thickness. For example, the elongation of samples of 3 mm thickness of melt D (CE= 4.49) show elongation values ranging from 23 to 29%. The reasons for this greater dispersion are not clear. The melts having CE<4.6% do not show exploded nodules or clustering. They show the presence of hypereutectic graphite nodules that are larger than the eutectic nodules. Nevertheless, such nodules appear to be evenly distributed along the sample's volume, and do not cause the strength and ductility of the material to drop below the minimum standardised values. Nevertheless, these larger nodules may account for the greater dispersion in the values of elongation.

Figure 23 shows the evolution of UTS and yield strength as a function of CE, for all samples tested. The yield strength remains approximately unchanged, while the UTS drops as CE exceeds 4.6%. This drop in UTS, which is accompanied by a drop in elongation, as shown above, is also caused by the presence of clusters of graphite nodules in the melts of very high CE.

5. Conclusions

Highly hypereutectic ductile irons (CE>4.6%) cast in thin wall sections show a marked tendency towards forming exploded graphite and graphite clustering.

Hypereutectic ductile irons of CE<4.6% show a proportion of large graphite nodules, typical of ductile iron. These larger nodules distribute homogeneously throughout the volume of the sample.

The degeneration of graphite morphology observed in highly hypereutectic irons is accompanied by a noticeable decrease in elongation.

Hypereutectic ductile irons of CE<4.6% usually satisfy the minimum elongation and strength values prescribed by ASTM A536.

REFERENCES

1) R. Martínez, R. Boeri and J. Sikora: Proc. of 2002 World Conference on ADI, AFS Publications, USA, (2002), 143.
2) D. M. Stefanescu, L. P. Dix, R. E. Ruxanda, C. Corbitt and T. S Piwonka: *AFS Trans.*, **110** (2002), 1149.
3) D. M. Stefanescu, R. E. Ruxanda and L. P. Dix: *Int. J. Cast Metals Res.*, **16** (2003), 319.
4) A. Javaid, J. Thomson, M. Sahoo and G. Davis: *AFS Trans.*, **109** (2001).
5) A. Javaid, J. Thomson, M. Sahoo and G. Davis: *AFS Trans.*, **107** (1999), 441.
6) C. Labrecque and M. Gagne: *AFS Trans.*, **108** (2000), 31.
7) O. N. Dógan, K. K. Schems and J. A. Hawk: *AFS Trans.*, **111** (2003), Paper 03-136.
8) A. Giacopini, R. Boeri and J. Sikora: *Mater. Sci. Technol.*, **19** (2003), 1755.
9) C. Labrecque, M. Gagne, A. Javaid and M. Sahoo: *Int. J. Cast Metals Res.*, **16** (2003), 313.
10) A. Javaid, K. G. Davis and M. Sahoo: *AFS Trans.*, **108** (2000), 191.
11) L. P. Dix, R. Ruxanda, J. Torrance, M. Fukumoto and D. M. Stefanescu: *AFS Trans.*, **111** (2003), Paper 03-109.
12) C. R. Loper Jr. and R. M. Kotschi: *AFS Trans.*, **82** (1974), 226.
13) R. E. I. Ruxanda, D. M. Stefanescu and T. Piwonca: Proc. Int. Conf. on the Science of Castings and Solidification, ed. by Lux Libris, Brasov, Romania, (2001), 361.